PHASE DIAGRAM, SOLIDIFICATION AND HEAT TREATMENT OF ALUMINUM ALLOYS

C. SIGLI, L. MAENNER, C. SZTUR and R. SHAHANI

Pechiney Centre de Recherches de Voreppe, BP 27, 38340 Voreppe, France.

ABSTRACT A method, based on the solubility product concept, is proposed in order to calculate phase diagram equilibria in hypo-eutectic and hypo-peritectic aluminum alloys. This method requires less adjustable parameters than common thermodynamics software and allows a faster assessment of multicomponent alloys. The accuracy of the approach is demonstrated by several examples. Moreover, a long-range diffusion routine has been developed and coupled with the equilibrium routine. Several applications are presented: quantification of back-diffusion during solidification, dissolution kinetics of eutectic intermetallic compounds and microstructural evolution during a brazing treatment.

Keywords: Phase Diagrams, Multicomponent Alloys, Solidification, Diffusion, Dissolution, Brazing

1. INTRODUCTION

Calculation of phase equilibria in multicomponent systems is at present a well mastered exercise which can be treated by several software [1, 2]. Among the most well known are Chemsage [3], MTDATA [4] and Thermo-Calc [5]. Each of these software minimizes the total alloy Gibbs energy at a given composition and temperature. This minimization relies on the description of the Gibbs energy of each phase expressed as a function of phase composition and temperature. These approaches are very general and can treat any phase diagram topologies; a review of their applications in the aluminum industry is given in [6].

The first objective of this paper is to present an alternate simplified model which is based on the concept of solubility product [7, 8, 9]. The method is particularly suited for an industrial research center and allows quick assessments of phase equilibria in aluminum alloys. To the authors' best knowledge, the simplicity and efficiency of the approach do not however preclude the high accuracy required for practical industrial applications. At present, the model can treat hypo-eutectic and hypo-peritectic Al-Mg-Si-Cu-Zn-Mn-Fe-Zr-Cr-Ti alloys.

The second objective of this paper is to demonstrate some industrial applications obtained by coupling the phase diagram routine with a very general long-range diffusion routine. By "long-range", we mean that nucleation, growth/dissolution and coarsening of precipitates are not taken into account and that each volume element in an alloy is supposed to be in local equilibrium. The coupling between the internally developed equilibrium routine and the diffusion subroutine does not present any difficulty; this is not always the case when dealing with commercial software for which the source files are not available [10]. The routines have been incorporated into a PC software with a friendly computer interface that can be used by non-experts. Several examples will be illustrated: back-diffusion during solidification, dissolution kinetics of eutectic intermetallic compounds and microstructural evolution during a brazing treatment.

2. PHASE DIAGRAM CALCULATION

2.1 The concept of product of solubility

The general expression of the molar Gibbs free energy of a solid solution in a regular solution model is given by the following expression:

$$G^{\alpha} = \sum_{i} \sum_{j,j>i} x_i^{\alpha} x_j^{\alpha} \Omega_{ij}(T) + RT \sum_{i} x_i^{\alpha} \ln\left(x_i^{\alpha}\right) \tag{1}$$

where the fcc structure is the reference structure and where the following notations have been used:

x_i^{α} atomic concentration of element i in the aluminum solid solution,
T temperature (in Kelvin),
$\Omega_{ij}(T)$ interaction parameter between elements i and j (J/mole); it may be written as $\Omega_{ij}(T) = A_{ij} + B_{ij} T$ with A_{ij} and B_{ij} constant.

The chemical potentials of elements are derived by the general equation:

$$\mu_i^{\alpha} = \frac{\partial G^{\alpha}}{\partial x_i^{\alpha}} + G^{\alpha} - \sum_{j} x_j^{\alpha} \frac{\partial G^{\alpha}}{\partial x_j^{\alpha}} \tag{2}$$

For the solid solution, Eq.2 becomes:

$$\mu_i^{\alpha} = RT \ln\left(x_i^{\alpha}\right) + \sum_{j,j\neq i} \Omega_{ij}(T) x_j^{\alpha} - \sum_{j} \sum_{k>j} \Omega_{jk}(T) x_j^{\alpha} x_k^{\alpha} \tag{3}$$

The Gibbs free energy for a compound P is expressed by the simple equation:

$$G^{P} = \sum_{i} x_i^{P} \mu_i^{P} = \Delta H_f^{P} - T \Delta S_f^{P} \tag{4}$$

The aluminum solid solution is in equilibrium with a stoechiometric compound P when the chemical potentials of each element in the solid solution and in the compound are equal. The following expression is then deduced:

$$\sum_{i} x_i^{P} \mu_i^{P} = \sum_{i} x_i^{P} \left\{ RT \ln\left(x_i^{\alpha}\right) + \sum_{j,j\neq i} \Omega_{ij}(T) x_j^{\alpha} - \sum_{j} \sum_{k>j} \Omega_{jk}(T) x_j^{\alpha} x_k^{\alpha} \right\} = \Delta H_f^{P} - T \Delta S_f^{P} \tag{5.a}$$

or

$$\prod_{i} \left(x_i^{\alpha}\right)^{x_i^{P}} = e^{\left\{ \frac{\Delta H_f^{P} - T\Delta S_f^{P} - \sum_{i} \sum_{j,j\neq i} \Omega_{ij}(T) x_j^{\alpha} x_i^{P} + \sum_{j} \sum_{k>j} \Omega_{jk}(T) x_j^{\alpha} x_k^{\alpha}}{RT} \right\}} \tag{5.b}$$

For an ideal solution, $\Omega_{ij}(T) = 0$ and Eq.5.b simplifies to:

$$\prod_{i} \left(x_i^{\alpha}\right)^{x_i^{P}} = K_P(T) = e^{\left\{ \frac{\Delta H_f^{P} - T\Delta S_f^{P}}{RT} \right\}} \tag{6.a}$$

For a sufficiently dilute regular solid solution, $x_{Al}^{\alpha} \approx 1, x_{i,i\neq Al}^{\alpha} \approx 0$ and Eq 5.b simplifies to:

$$\prod_{i} \left(x_i^{\alpha}\right)^{x_i^{P}} = K_P(T) = e^{\left\{ \frac{\left(\Delta H_f^{P} - \sum_{i\neq Al} x_i^{P} \Lambda_{Al-i}\right) - T\left(\Delta S_f^{P} + \sum_{i\neq Al} x_i^{P} B_{Al-i}\right)}{RT} \right\}} \tag{6.b}$$

In both cases, ideal or dilute regular solid solutions, the logarithm of the equilibrium solubility product is predicted to vary linearly with 1/T. This behavior is observed for aluminum alloys [7, 9] and is illustrated for some compounds in Fig.1.

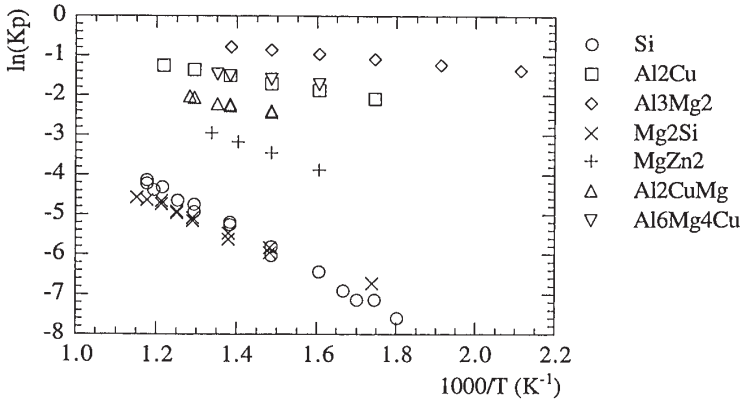

Fig.1: *Illustration of the solubility product concept for several compounds in equilibrium with the aluminum solid solution. Experimental data are taken from [11, 12].*

2.2 Equilibrium between the aluminum solid solution and a set of stoechiometric compounds

For each element "i", the concentrations in solid solution, x_i^α, are related to the alloy compositions, x_i^o, as well as the compounds' atomic fraction and concentrations (f_P and x_i^P respectively) by the following mass balance equation:

$$x_i^o = x_i^\alpha \times \left\{1 - \sum_P f_P\right\} + \sum_P f_P \, x_i^P \tag{7}$$

For a given temperature and alloy composition, the equilibrium is easily obtained by a dichotomy method on the compounds' fraction while applying the following reaction rules:

$\prod_i \left(x_i^\alpha\right)^{x_i^P} < K_P(T)$: dissolution of compound P

$\prod_i \left(x_i^\alpha\right)^{x_i^P} > K_P(T)$: precipitation of compound P

$\prod_i \left(x_i^\alpha\right)^{x_i^P} = K_P(T)$: equilibrium of the compound P with the solid solution (Eq.8, no reaction)

The calculation is stopped when all the coexisting compounds are in equilibrium with the aluminum solid solution (i.e. Eq.8 is fulfilled within a given error). Non-stoechiometric compounds are treated as a set of stoechiometric compounds and the above mentioned algorithm still applies.

2.3 Case of the liquid phase

To keep the model simple, the liquid phase has not been treated rigorously. An empirical approach has been adopted where the solidus temperature, T_{sol}, and the partition coefficient of each element, k_i, are fitted by a polynomial expansion of the solid solution concentration, x_i^α. The liquid concentration, x_i^L, is then simply given by the relation:

$$x_i^L = \frac{x_i^\alpha}{k_i} \tag{8}$$

This formalism enables a treatment of the liquid phase analogous to the treatment of the compounds; the following reaction rules can be used:

$T_{sol}\left(\{x_i^\alpha\}\right) < T$: the liquid phase increases its atomic fraction,

$T_{sol}\left(\{x_i^\alpha\}\right) > T$: the liquid phase decreases its atomic fraction,

$T_{sol}\left(\{x_i^\alpha\}\right) = T$: the liquid phase is in equilibrium with the solid solution (no reaction).

2.4 Examples of phase diagram calculation

Examples of phase diagram calculations are given in Figs.2-3. To the authors' best knowledge, the simplified formalism presented in the former paragraphs is sufficient to give an accurate description of the Al-Mg-Si-Cu-Zn-Mn-Fe-Zr-Cr-Ti phase diagram in the aluminum rich corner. At present, the database includes the thermodynamic description of 18 stoechiometric and 7 non-stoechiometric compounds.

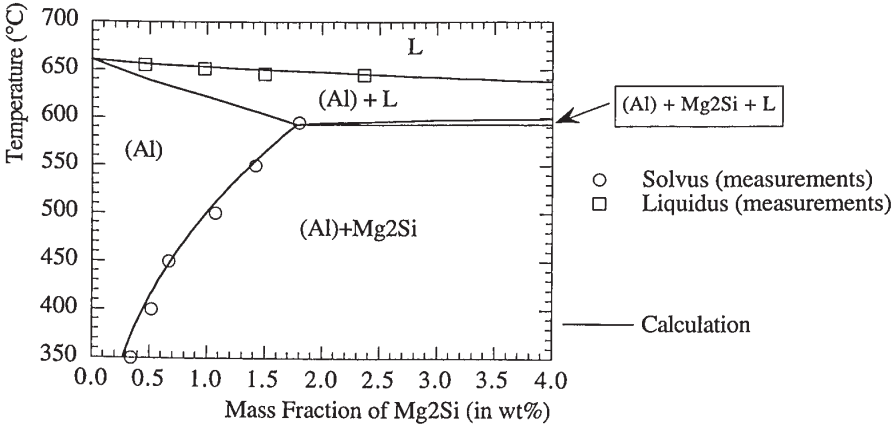

Fig.2: *Calculated quasi-binary phase diagram along the Al-Mg_2Si axis. Measurements are taken from [12] for the solvus and from [13] for the liquidus.*

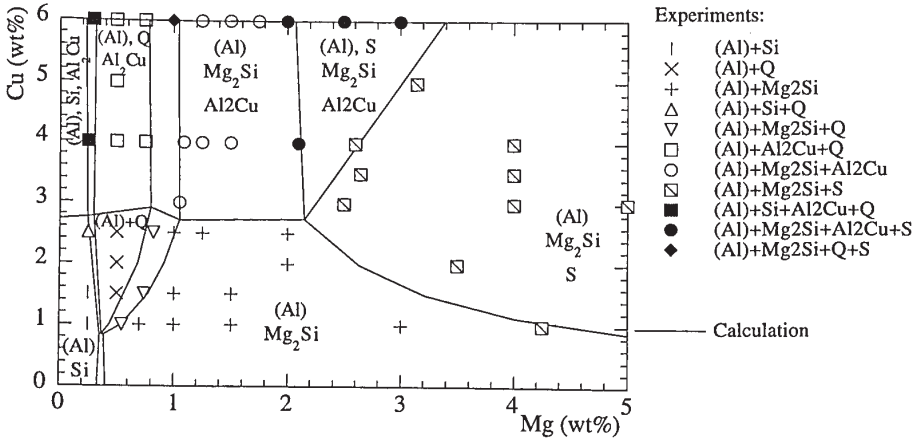

Fig.3: *Calculated Al-Cu-Mg-Si phase diagram at 460°C for a constant 0.6 wt% composition of Silicon. Measurements are taken from [14].*

3. PREVISION OF SOLIDIFICATION PATH, SOLIDIFICATION CURVES AND MICROSEGREGATIONS DURING CASTING

3.1 Scheil Model

The simplest model to simulate solidification path (liquid concentration evolution), solid fraction versus temperature curves and microsegregation during casting is the Scheil model [15]. The assumptions are threefold: equilibrium at the liquid/solid interface, no diffusion in the solid phases and infinite diffusion in the liquid phase. The coupling of a Scheil solidification routine with a phase diagram subroutine is straightforward and proceeds as follows. The temperature is first set equal to the liquidus temperature corresponding to the alloy composition. It is then decreased by a small decrement and the equilibrium is calculated. The alloy composition is then set equal to the liquid composition, the temperature decreased again by a small decrement and the equilibrium calculated again. This process is iterated until no liquid is found at equilibrium. The software stores the intermediate liquid ($x_i^L(s)$) and solid phase ($x_i^\alpha(s)$) concentrations as well as phase fractions ($F_p(s)$) at each iterative step "s".

The global residual liquid fraction left after step "s" is given by:

$$f_L(s) = \prod_{k=1}^{s} F_L(k) \tag{9}$$

The cumulative fraction of each solid phase (compound p or aluminum solid solution α) formed after step "s" is calculated by the equation:

$$f_p(s) = \sum_{k=1}^{s} F_p(k) \times f_L(k-1) \tag{10}$$

3.2 Solidification with back-diffusion in the Aluminum solid solution

For fast diffusing atoms in the aluminum solid solution, like Magnesium, Silicon, Copper and Zinc, a more accurate treatment consists in evaluating, at each iterative step "s", the amount of back-diffusion occurring in solid solution. This is done by using a finite difference scheme, by assuming local equilibrium in each volume element of secondary dendrite arms, by calculating the solute concentration in each volume element (i.e. applying the phase diagram subroutine for the current temperature and the local alloy concentration) and by solving Fick's laws. The diffusion matrix in the aluminum solid solution is assumed to be diagonal; values for the diagonal terms are taken from literature [16, 17]; they are presented in Fig.4.

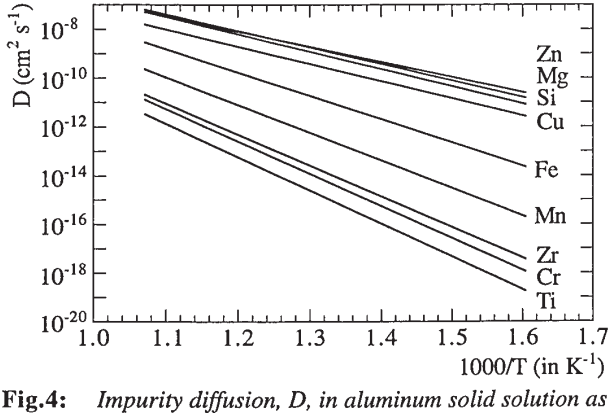

	Do (cm2 s-1)	Q (kJ mol-1)
Mg	1.24	130.4
Si	2.02	136
Cu	0.654	136.1
Zn	0.25	119.6
Fe	53	183.4
Mn	317	217
Cr	1850	253
Zr	728	242
Ti	1120	259.8

$$D = D_0 \times e^{-\frac{Q}{RT}}$$

Fig.4: *Impurity diffusion, D, in aluminum solid solution as a function of temperature (taken from [16], except for Ti [17]).*

The secondary dendrite arm spacing (sdas) is an important input data in diffusion calculations. It depends strongly on the cooling rate and, to a lesser extent, on alloy composition [18, 19]. Some attempts have been made in the past to predict the sdas [20, 21, 22]. These models are very useful to understand the physics behind variations of the sdas; their results, however, are not accurate enough to be used as input parameters for diffusion calculations. In practice, measured sdas are used.

An example of calculated solid fraction versus temperature curve is given in Fig.4 for aerospace alloy 7010. Thermal analysis measurements (for example, see [18]) have been performed on the same alloy; they are compared with calculations in Fig.5. As can be seen, if back-diffusion is taken into account, a good agreement is observed between experiments and calculations. A test of the accuracy of the model has also been performed on some common foundry alloys; the results are presented in Fig.7. These predictions are used as input parameters for our casting simulation program (PAM-CAST™ / SIMULOR®) [23]. This program, based on Navier-Stokes equations coupled with thermal equations, predicts filling behavior and solidification of cast parts.

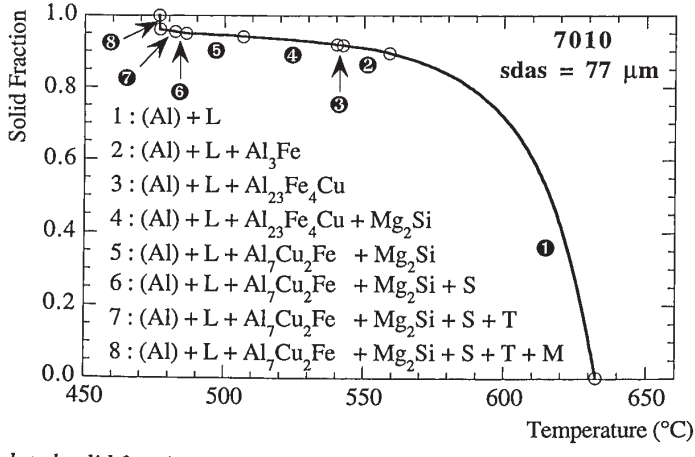

Fig.5: *Calculated solid fraction versus temperature curve for alloy AA 7010; the predicted crystallization sequence is also indicated.*

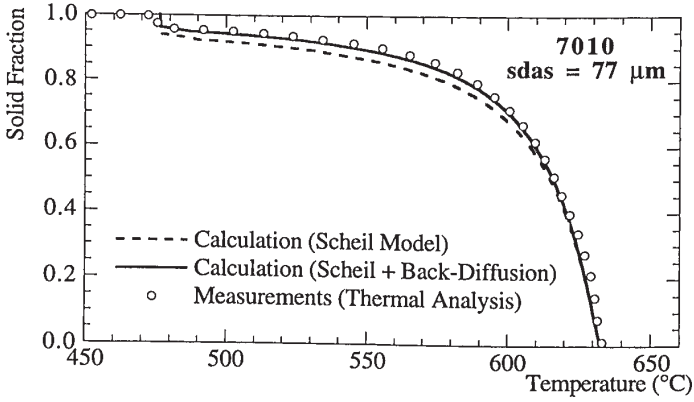

Fig.6: *Comparison between calculated and experimental solidification curves. Calculations have been carried out with a simple Scheil Model or by taking into account back-diffusion of solute atoms in the aluminum solid solution.*

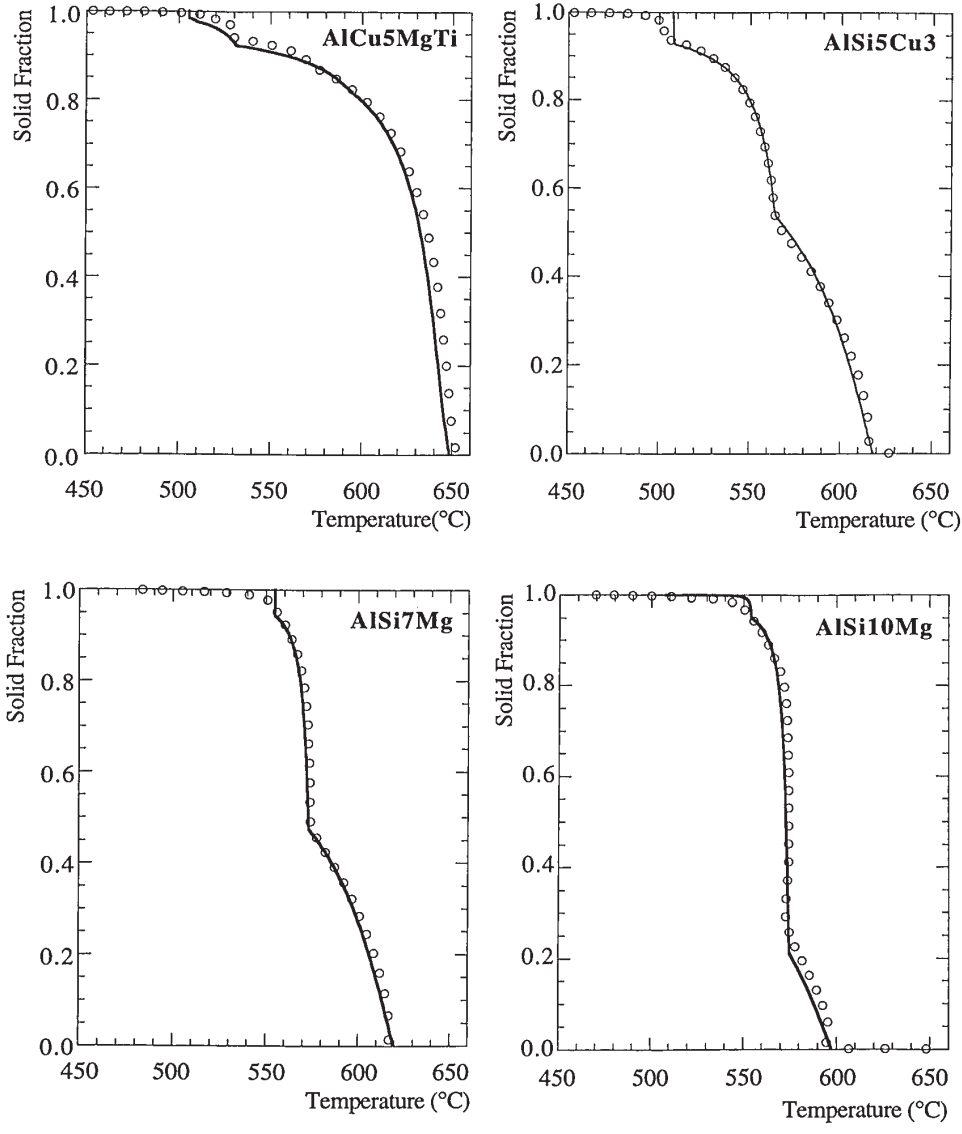

Fig.7: *Comparison between calculated (full line) and experimental (circles) solid fraction-temperature curves for typical foundry aluminum alloys. Measurements were performed by thermal analysis (for example, see [18]).*

4. LONG-RANGE DIFFUSION IN ALUMINUM ALLOYS

The model presented in §3.2 assumes local equilibrium in each volume element of the dendrite and assumes that nucleation and growth/dissolution are very fast. This assumption seems reasonable when simulating dissolution kinetics of eutectic intermetallic compounds or microstructure evolution during brazing. Following are some examples of the application of this model.

4.1 Dissolution kinetics of eutectic intermetallic compounds

For binary alloys, the calculation scheme presented in §3.2 becomes identical to the successful finite difference approach proposed in the past to simulate the dissolution kinetics of Al_2Cu eutectic compounds [24, 25]. The predicted dissolution kinetics of an as-cast Al-4.5 wt% copper is presented in Fig.8.

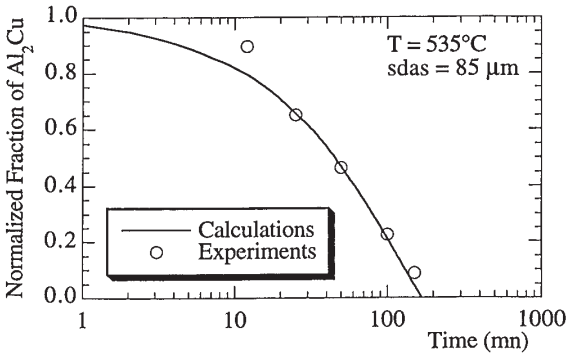

Fig.8: *Comparison between calculated and experimental dissolution kinetics of Al_2Cu compounds. The experimental data, including the sdas measurement, are taken from [24].*

The present calculation scheme can treat complex industrial alloys containing as many solute elements as desired provided the corresponding phase diagram has been assessed. An example is given in the next paragraph.

4.2 Brazing simulation

The kinetic model has been applied in order to understand the microstructure evolution occurring in AA3005 alloy (Si:<0.6, Fe<0.7, Cu<0.3, 1<Mn<1.5, 0.2<Mg<0.6, Cr<0.1) clad with AA4045 (9<Si<11, Fe<0.8, Cu<0.3, Mn<0.1, Mg<0.1) during a brazing treatment (5 mn at 595°C). These alloys are used for automotive heat exchangers. During the brazing treatment, the 4045 clad melts and joins the components while silicon diffuses from the liquid clad to the solid core material and provokes the precipitation of manganese in the clad/core interlayer. It is reported that the dense precipitated interlayer is more anodic by approximately 20 mV compared to the core material and protects the core material from corrosion [26]. The kinetic model reproduces the observed microstructure gradients (see Fig 9.a-b). The calculated gradients have been coupled with a simple model that relates linearly the corrosion potential to solute concentrations in the matrix. The coefficients of the linear equation were adjusted from measurements reported in Ref.[27]. A potential difference of 12 mV between the interlayer and the core was calculated (see Fig.9.c); it is in reasonable agreement with the measurement [26].

Magnesium is added to 3005 to improve mechanical properties; it is however well known that excessive magnesium levels can lead to brazing problems in the case of Controlled Atmosphere Brazing (CAB). The concentration of magnesium in the 4045 cladding can be predicted and controlled by using the present model (see Fig.9.d).

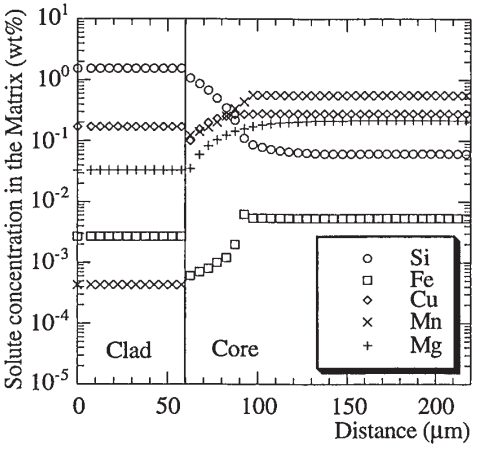

a : *Solute concentration gradient in the aluminum matrix*

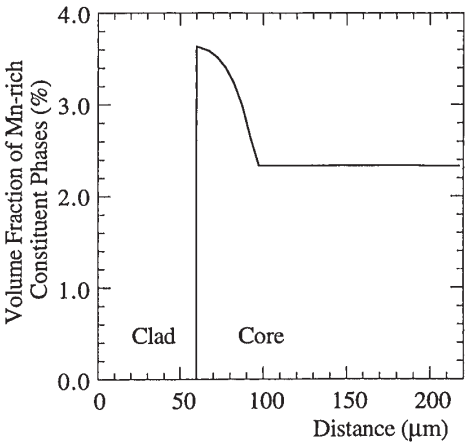

b : *Volume fraction gradient of manganese-rich constituent phases*

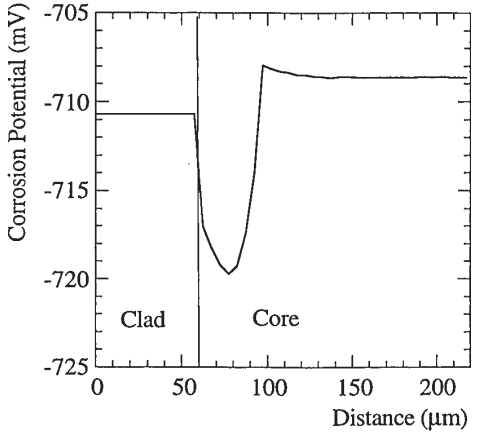

c : *Corrosion potential gradient*

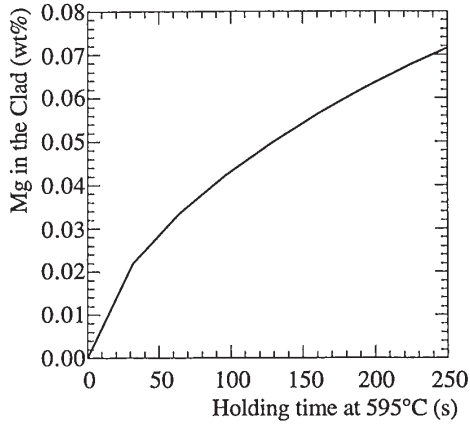

d: *Predicted evolution of the average magnesium concentration in the clad as a function of holding time at 595°C.*

Fig.9 *Predicted microstructure and corrosion potential gradient across the clad-core material after a brazing treatment of 5 mn at 595 °C followed by a quench. The clad alloy is AA4045 whereas the core is made of AA3005.*

5 CONCLUSIONS AND PERSPECTIVES

The phase diagram, solidification and long-range diffusion routines have been incorporated into a friendly PC software which can be used by a thermodynamics non-expert. The solubility product concept allows a quick and accurate assessment of phase diagrams in the aluminum rich corner; it also accelerates calculations. The dissemination of the software enables industrial research engineers to exploit easily the Al-Mg-Si-Cu-Zn-Mn-Fe-Zr-Cr-Ti phase diagram while sharing a common internal "phase diagram culture". By doing so, the predictions of the software are constantly compared with microstructural measurements performed in research projects; if necessary the thermodynamic database is upgraded. The phase diagram, solidification and long-range diffusion routines are now in the process of being implemented in the integrated metallurgical simulators for heat-treatable and non-heat-treatable aluminum alloys [28, 29, 30] bringing new prospects for material and process control of aluminum alloys. These routines are also being currently used, together with thermo-mechanical routines, in order to understand and predict materials behavior during solidification or welding.

The tasks that are most frequently asked of the thermodynamic and kinetic software are the prediction of:
- the liquidus and solidus temperature,
- the solidification curve (solidified fraction as a function of temperature),
- the composition and temperature allowing the complete dissolution of one or several intermetallic compounds,
- the determination of hypo-eutectic and hypo-peritectic domains,
- the dissolution kinetics of intermetallic compounds formed during solidification,
- the microstructural evolution during brazing.

The present kinetic model simulates "long-range" diffusion; it relies on the assumption of local equilibrium in each alloy volume element. In order to relax this assumption, work is under way in order to develop a general formalism describing, with a coherent set of equations, the rate of nucleation, growth/dissolution and coarsening of a set of compounds having different compositions in a multicomponent alloy.

ACKNOWLEDGEMENTS

The authors would like to thank Pechiney Rhenalu and Aluminium Pechiney for financing this study.

REFERENCES

1. U.R. Kattner, "The Thermodynamic Modelling of Multicomponent Phase Equilibria", JOM **49**, 14-19 (1997).

2. T. Kraft, Y.A. Chang, "Predicting Microstructure and Microsegregation in Multicomponent Alloys", JOM **49**, 20-28 (1997).

3. E. Königsberger, G. Eriksson, "A new optimization routine for ChemSage", CALPHAD **19**, 207-214 (1995).

4. R.H. Davies, et al., "Thermodynamic Modelling Using MTDATA, A Description Showing Applications Involving Oxides, Alloys and Aqueous Solutions", Applications of Thermodynamics in the Synthesis and Processing of Materials, P. Nash, B. Sundman, Eds. (TMS, 1995) pp. 371-384.

5. B. Sundman, B. Jansson, J.O. Andersson, "The Thermo-Calc Databank System", CALPHAD **9**, 153-190 (1985).

6. B. Dubost, "Industrial applications and determination of equilibrium phase diagrams for light alloys. Progress and prospects", La Revue de Métallurgie-CIT/ Science et Génie des Matériaux 195-209 (1993).

7. R.H. Brown, L.A. Willey, "Constitution of Alloys", Aluminum, K. R. V. Horn, Ed. (ASM, 1967), vol. I, pp. 32-54.

8. D.A. Porter, K.E. Easterling, "Phase Transformations in Metals and Alloys (2nd Ed.)", (Chapman&Hall, 1992).

9. N. Ryum, "Physical Metallurgy of Heat Treatable Alloys" in Aluminum Alloys: Their Physical and Mechanical Properties, E. A. Starke, T. H. Sanders (Eds.), Charlottesville, USA, 1986, vol. III, pp. 1511-1545.

10. P. Kolby, "Applications of Thermodynamically Modelled Phase Diagram Data in Mathematical Modelling of Industrial Processes" in Aluminum Alloys: Their Physical and Mechanical Properties (ICAA5), J. Driver (Ed.), Grenoble, France, 1996, vol. 2, pp. 661-666.

11. M. Hansen, "Constitution of binary alloys", Metallurgy and Metallurgical Engineering Series (McGraw-Hill, 1958).

12. H.W.L. Phillips, "Annotated Equilibrium Diagrams of Some Aluminum Alloy Systems", Monograph and Report Series (Institute of Metals, 1959), vol. 25.

13. E.H. Dix, F. Keller, R.W. Graham, "Equilibrium Relations In Aluminium-Magnesium Silicide Alloys of High Purity", Trans. A.I.M.M.E. Inst. Metals Div. 404-420 (1931).

14. H.J. Axon, "Equilibrium Relations at 460°C in Aluminium-Rich Alloys Containing 0-7% Copper, 0-7% Magnesium and 0.6% Silicon", J. Inst. Metals **81**, 209 (1952-53).

15. E. Scheil, "Bemerkungen zur Schlichtkristallbildung", Z. Metallk. **34**, 70-72 (1942).

16. H. Bakker, "Diffusion in Solid Metals and Alloys", Landolt-Börnstein (Springer-Verlag, Berlin, 1990), vol. 26.

17. G. Rummel, T. Zumkley, M. Eggersmann, K. Freitag, H. Mehrer, "Diffusion of Implanted 3d-Transition Elements in Aluminium; Part I: Temperature Dependence", Z. Metallkd. **86**, 122-130 (1995).

18. L. Bäckerud, E. Krol, J. Tamminen, "Solidification Characteristics of Aluminium Alloys", (Skanaluminium, 1986), vol. Volume 1: Wrought Alloys.

19. L. Bäckerud, G. Chai, J. Tamminen, "Solidification Characteristics of Aluminium Alloys", (AFS/Skanaluminium, 1990), vol. Volume 2: Foundry Alloys.

20. D.H. Kirkwood, "A Simple Model for Dendrite Arm Coarsening During Solidification", Mat. Sci. Eng. **73**, L1-L4 (1985).

21. U. Feurer, R. Wunderlin, "Einfluß der Zusammensetzung und der Erstarrungsbedingungen and die Dendritenmorphologien binärer Al-Legierungen", Fachbericht der Deutschen Gesellschaft für Metallkunde, Oberursel, FRG, 1977).

22. T.Z. Kattamis, J.C. Coughlin, M.C. Flemings, "Influence of Coarsening on Dendrite Arm Spacing of Aluminum-Copper Alloys", Trans. Met. Soc. AIME **239**, 1504-1511 (1967).

23. P. Laty, P. Large, C. Rigaut, "Simulor, a Software to Help the Development of the Mold" in 18th Annual Automotive Materials Symposium, Detroit, USA, 1991.

24. S.N. Singh, B.P. Bardes, M.C. Flemings, "Solution treatment of cast Al-4.5 pct Cu Alloy", Met. Trans. **1**, 1383-1388 (1970).

25. A. Roosz, Z. Gacsi, G. Fuchs, "Solute Redistribution During Solidification and Homogenization of Binary Solid Solution", Acta metall. **10**, 1745-1754 (1984).

26. G.J. Marshall, A.J.E. Flemming, A. Gray, R. Llewellyn, "Development of a Long Life Aluminium Brazing Sheet Alloy" in Aluminum Alloys: Their Physical and Mechanical Properties (ICAA4), T. H. Sanders, E. A. Starke (Eds.), Atlanta, USA, 1994, vol. I, pp. 467-474.

27. E.H. Hollingsworth, H.Y. Hunsicker, "Corrosion of Aluminum and Aluminum Alloys", Metal Handbook (9th Edition), Corrosion, (ASM International, 1987), vol. 135, pp. 583-609.

28. C. Sigli, H. Vichery, B. Grange, "Computer Assisted Metallurgy For Packaging Alloys" in Aluminum Alloys For Packaging II, J. G. Morris, S. K. Das, H. S. Goodrich (Eds.), Anaheim, USA, 1996, pp. 189-197.

29. C. Sigli, H. Vichery, B. Grange, "Computer Assisted Metallurgy for Non-Heat Treatable Aluminum Alloys" in Aluminum Alloys: Their Physical and Mechanical Properties (ICAA5), J. Driver (Ed.), Grenoble, France, 1996, vol. I, pp. 391-396.

30. P. Sainfort, C. Sigli, G.M. Raynaud, Ph. Gomiero, "Structure and Property Control of Aerospace Alloys" in Aluminum Alloys: Their Physical and Mechanical Properties (ICAA5), J. Driver (Ed.), Grenoble, France, 1996, vol. 4, pp. 25-32.